1   **Nordic Snow Radar Experiment**

3   **Juha Lemmetyinen[1], Anna Kontu[1], Jouni Pulliainen[1], Juho Vehviläinen[1], Kimmo**

4   **Rautiainen[1], Andreas Wiesmann[2], Christian Mätzler[2], Charles Werner[2], Helmut**

5   **Rott[3], Thomas Nagler[3], Martin Schneebeli[4], Martin Proksch[4], Dirk Schüttemeyer[5],**

6   **Michael Kern[5] and Malcolm Davidson[5].**

7   [1]{Finnish Meteorological Institute, Finland}

8   [2]{GAMMA Remote Sensing and Consulting AAG, Switzerland}

9   [3]{ENVEO IT GmbH, Austria}

10   [4]{WSL Institute for Snow and Avalanche Research SLF, Switzerland}

11   [5]{ESA-ESTEC, the Netherlands}

13   Correspondence to: Juha Lemmetyinen (juha.lemmetyinen@fmi.fi)

15   **Abstract**

16   The objective of the Nordic Snow Radar Experiment (NoSREx) campaign was to provide a

17   continuous time series of active and passive microwave observations of snow cover in a

18   representative location of the Arctic boreal forest area, covering a whole winter season. The

19   activity was a part of Phase A studies for the ESA Earth Explorer 7 candidate mission

20   CoReH2O (Cold Regions Hydrology High-resolution Observatory).

21   The NoSREx campaign hosted two main microwave instruments; a frequency scanning

22   scatterometer operating on frequencies from X- to Ku band, and a microwave dual-polarization

23   radiometer system operating from X- to W bands. In situ measurements consisted of manual

24   snow pit measurements at the main test site as well as extensive automated measurements on

25   snow, ground and meteorological parameters.

1   This study provides a summary of the obtained data, detailing measurement protocols for
2 both microwave instruments and in situ reference data. A first analysis of the microwave
3 signatures against snow parameters is given.

4   All data, including the raw data observations, are available through the European Space Agency
5 and the Finnish Meteorological Institute for research purposes. A consolidated dataset of
6 observations, comprising of the key microwave and in situ observations, is provided through
7 the ESA campaign data portal to enable easy access to the data.

9 **1   Introduction**

10   Knowledge on the duration, extent and total mass of seasonal snow cover is crucial for
11 hydrological forecasts, numerical weather prediction and estimation of the energy balance of
12 the Earth (Groisman et al., 1994; Brasnett, 1999; Barnett et al., 2005). Seasonal snow cover is
13 also a strong indicator of global climate change (Derksen and Brown, 2012). The scarcity of
14 observation networks makes data collected *in situ* unreliable for Arctic and boreal areas, making
15 Earth Observation from satellites an appealing option. The extent of seasonal snow cover can
16 be retrieved with high spatial accuracy using both optical and radar sensors. Methods for
17 retrieving snow mass, or snow water equivalent (SWE), presently rely on passive microwave
18 sensors (Kelly et al., 2003; Takala et al., 2011). Although these provide good global coverage
19 and a long history of observations, present products suffer in accuracy from the inherent coarse
20 spatial resolution of passive microwave sensors over inhomogeneous areas.

21   Providing high-resolution information on the mass of seasonal snow cover was the main
22 objective of CoReH2O (Cold Regions Hydrology High-Resolution Observatory), a candidate
23 mission for the European Space Agency's 7th Earth Explorer (ESA, 2012). The payload of
24 CoReH2O was envisaged as a dual-polarized, dual-frequency (X and Ku band) synthetic
25 aperture radar (SAR), with the capability of detecting SWE, as well as snow accumulation on
26 glaciers, at spatial resolutions ranging from 200 to 500 m (Rott et al., 2012). In order to support
27 the development of geophysical retrieval algorithms for CoReH2O, the NoSREx (Nordic Snow
28 Radar Experiment) was initiated by ESA in 2009. The aim of the campaign was to collect near-
29 continuous observations of snow cover radar signatures in the boreal forest/taiga region using
30 a tower-based configuration, supported by frequent in situ observations. The campaign was
31 designed to cover entire winter periods from snow free conditions to eventual snow melt-off.
32 With several extensions, the collected dataset for NoSREx covers a total of four snow seasons

1 from 2009 to 2013. The campaign was conducted at the Finnish Meteorological Institute Arctic

2 Research Centre (FMI-ARC) in Sodankylä, Finland. The radar backscatter measurements were

3 complemented by multi-frequency microwave radiometer observations and numerous in situ

4 observations of snow, soil and atmospheric properties, using both manual and automated

5 methods. Advanced methods for quantifying the snow microstructure were implemented on a

6 campaign basis. The campaign provides a unique, near-continuous dataset of coinciding active

7 and passive microwave observations of snow cover and diverse measurements of snow

8 characteristics. During the las two seasons, airborne acquisitions using the ESA SnowSAR

9 instrument were made over the area in order to analyse spatial variability of backscattering and

10 to demonstrate the CoReH2O mission concept (see e.g. ESA 2012; Lemmetyinen et al., 2014).

11 However, these data are not presented here.

12   Data collected during NoSREx have found use in numerous recent studies exploring the

13 modelling of microwave signatures of snow covered terrain. Here, we provide an overview of

14 the used instrumentation, data acquisition protocols and the collected microwave signatures.

15 The calibration accuracy of the various instrumentation is discussed. We also give

16 recommendations and suggestions on how in situ data could be used optimally to support

17 analysis of microwave observations. We discuss recent studies which have already exploited

18 the results of the campaign, and give recommendations for future experimental campaigns on

19 snow microwave signatures.

2   Description of experiment setup

2.1   Measurement location

23   The main test site of NoSREx, the Intensive Observation Area (IOA), was located on a forest

24 clearing surrounded by a sparse spruce/pine dominated forest. The site, as well as the area at

25 large, represents a typical boreal forest/taiga landscape. According to a soil composition survey.

26 soil at the IOA consisted of sand (70%), silt (29%) and clay (1%) with a thin organic surface-

27 layer (2 - 5 cm). The sparse ground vegetation consisted mainly of lichen and heather and other

28 small vegetation typical for the boreal forest region. Small trees and bushes estimated to

29 influence e.g. snow accumulation were manually removed from the site in autumn before the

30 onset of snow cover.

1 The main microwave instruments installed were the *SnowScat* scatterometer (Werner et al.,

2 2010) and the *SodRad* multi-frequency radiometer system. Data from an L-band instrument

3 (Schwank et al., 2010) is available from the same site, but these data are not discussed here. All

4 instruments were mounted on tower structures overlooking the forest clearing, allowing

5 partially to cover also same sectors of the test field, albeit at differing effective incidence angles.

6 Automated sensors were located adjacent to the test field, as was the main location for manual

7 snow measurements. The location of the microwave instrumentation, as well as the approximate

8 locations of various in situ sensors are depicted in Figure 1. The measurement protocols for

9 each instrument are described in detail in the following sections.

2.2   Microwave scatterometry

12 The *SnowScat* scatterometer, manufactured by Gamma Remote Sensing, is a frequency step

13 four-polarization scatterometer (VV, HH, VH and HV), operating between the frequency range

14 of 9.2 and 17.9 GHz (Werner et al., 2010). Equipped with a positioner device, the system allows

15 scanning in both azimuth and elevation. For NoSREx, the instrument was installed on a tower

16 structure at the height of 9.6 meters above ground overlooking the IOA. The instrument was set

17 to measure regular scans of the test field, first every three hours in 2009. The scan of the main

18 measurement sector (sector 1) comprised of 17 independent look directions in azimuth at four

19 incidence angles at 30, 40, 50 and 60 degrees. From the autumn of 2010, the scan interval was

20 increased to four hours to allow for scanning over an additional sector (sector 2) adjacent to the

21 main observation section (see Figure 1). The data presented in this study consists of calibrated

22 sigma nought values, averaged over the full azimuth scan of sector 1. Sector 2 data, however,

23 are included in the NoSREx consolidated datasets. The technical specifications of *SnowScat* are

24 given in Table 1.

25 *SnowScat* provided an internal calibration loop for compensation of internal temperature

26 changes. The calibration consistency was verified by measuring dedicated calibration targets

27 before and after each scan (a ~20 cm diameter sphere for all seasons, and for the third and fourth

28 seasons, an additional flat plate target enabling assessment of cross-pol accuracy). A typical

29 variability of co-polarized backscatter from the calibration sphere was measured to be less than

30 +/- 1dB.

1   The measurement protocol of *SnowScat* included two measurements of the calibration sphere

2   for reference purposes. In addition, the metal plate was measured for reference purposes during

3   NoSREx III and IV. The nominal scan sequence was

4   • Cal sphere measurement

5   • Plate measurement (for NosREx III and IV)

6   • Sector 1 scan

7   • Cal sphere measurement

8   • Plate measurement (for NosREx III and IV)

9   • Sector 2 scan (for NosREx II to IV)

11 **2.3   Microwave radiometry**

12 The *SodRad* system, including measurements at 10.65, 18.7, 21, 37 and 90 GHz (H and V

13 pol), was mounted on a 4.1 m-high platform overlooking the forest clearing. The 90 GHz

14 radiometer was available from 2009 until 2012, when it was replaced by the 21 GHz system.

15 Measurements were made by performing a scan in the elevation direction, resulting in ground

16 incidence angles from 30 to 70° off nadir, in steps of 5°. Although the system allowed scans in

17 azimuth, most measurements were made in a single azimuth direction. In order to avoid RFI

18 contamination in particular at the 10.65 and 18.7 GHz systems, the measurements were timed

19 to occur between scans of the *SnowScat* instrument. Thus, the elevation scan was performed

20 every three hours during 2009-2010, and every four hours in following winters. In between

21 elevation scans, *SodRad* was set to measure a fixed incidence angle (50 or 53 degrees,

22 depending on season). These data are available upon a separate request. The technical

23 specifications of SodRad are given in Table 2.

24 The measurement sequence of *SodRad* consisted of

25 • the elevation scan

26 • a measurement of the sky cold target reference at zenith (10 minutes)

27 • a fixed angle measurement (until next elevation scan)

28 The tower-based radiometers were calibrated using a two-point calibration with external

29 targets, using a microwave absorber at ambient temperature and a similar target cooled by liquid

30 nitrogen. Verification of calibration stability was performed using the cold sky reference at

31 zenith (imposing a minimal influence from changing atmospheric conditions) after each

1 elevation scan. Additional calibration experiments included measurements of external targets

2 before and after the campaign season, including absorber material cooled by liquid nitrogen.

3 Analysis of the cold sky measurements indicates a drift of less than < 2 K for all channels and

4 polarizations (using only measurements made under clear sky conditions). Absolute accuracy

5 of the calibration was estimated to be better than 1 K for the 18.7 and 36.5 GHz channels, and

6 better than 2 K for the 10.65 GHz channels. The increased uncertainty of the 10.65 GHz

7 channels is due to use of a large parabolic reflector in front of the antenna feed, whereas 18.7

8 and 36.5 GHz channels utilize horn antennas; the parabolic reflector exhibited some sidelobe

9 effects which could not be entirely removed in the calibration.

10 **2.4 Manual in situ data collection**

11   Manual snow observations consisted of weekly snowpit measurements. Snowpits were made

12 at a distance of ca. 10-20 meters from the radiometer footprints in the same measurement field

13 (Figure 1). Due to the destructive nature of snowpit measurements, consecutive pits were made

14 at a distance of 50-100 cm from the previous pit. Measured parameters included bulk snow

15 depth, density and SWE using a snow corer and manual scale, snow density profiles at 5 cm

16 intervals using a 250 cm^3 manual cutter and scale, snow temperature profile at 10 cm intervals

17 using a digital thermometer, an assessment of snow layering based on a manual assessment of

18 snow hardness variations, and snow grain size and type estimation. The snow grain size and

19 type were estimated visually from macro-photography of snow samples, taken against a 1-mm

20 reference grid. A grain size classification was made following Fierz *et al.* (2009); in addition,

21 the typical grain size (average maximum diameter of typical snow grains, referred to hereafter

22 as *E*) was estimated visually. One snow sample was taken from the centre of each identified

23 snow layer, and the estimated grain size of the sample was considered to be applicable for the

24 whole layer.

25   During the third and fourth campaign seasons, snow Specific Surface Area (SSA) was

26 measured with the IceCube instrument manufactured by A2 Photonic sensors, France. The

27 measurement is based on IR reflectance of a snow sample placed inside an integrating sphere

28 (Gallet et al., 2009). The vertical snow profile was sampled at 3 cm resolution, excluding hard-

29 packed layers which presented difficulties for sampling. The time series of SSA measurements

30 are not a part of the NoSREx consolidated datasets but are available on separate request.

31   As snow pit observations were not made directly in the footprint of microwave instruments,

32 with the exception of specific tests (see Proksch et al., 2015), the snow profile information

1   should be treated with caution. In addition to temporal variability, also the spatial variability of

2   snow should be considered. As this can be notable even at short distances, it is not

3   recommended to use the measured profiles as they are for direct estimation of snow properties

4   at the instrument footprints. Rather, e.g. Lemmetyinen et al. (2015) applied a simplification of

5   the measured snow profiles to either one or two layers. In addition, a third order fit was applied

6   to the observations of E to reduce uncertainty arising e.g. from observer bias.

2.5   Automated in situ data

9   Several automatic measurement instruments were installed at the IOA. Two acoustic sensors

10   were used to record snow depth (SD). One sensor was placed in the forest clearing near the

11   *SodRad* platform tower and another under the forest canopy at a distance of ca. 50 meters. Air

12   temperature (T_{air}) was measured at the same locations. Three automated soil moisture and soil

13   temperature measurement sensors were installed at different locations in the test field. Snow

14   Water Equivalent was measured directly with an experimental device (GWI, Gamma Water

15   Instrument). Data from other automated in situ observations were collected into the

16   consolidated datasets from the FMI sounding station (ca. 500 meters from the IOA) and

17   Meteorological mast, in the immediate vicinity of the IOA.

2.6   Intensive observation periods

19   Intensive Observation Periods (IOPs) were organized during the first three NoSREx

20   campaigns. The objective of the IOPs was to complement the collected time series of basic

21   observations, in particular by employing advanced methods for characterization of snow

22   microstructure. The measurements consisted of

23   • SSA analyses using Near-Infrared (NIR) photography (Matzl et al., 2006)

24   • Snow micropenetrometry using the Snow MicroPen, (SMP, Schneebeli et al., 1998;

25   Proksch et al., 2015)

26   • Computer Tomography (CT) analysis of casted snow samples (Matzl et al., 2010)

27   .In particular, the measurements provide a means to validate visual estimations of layering

28   against SMP profiles, validate and compare visual grain size estimates against correlation

29   length from CT imagery, validate density profile measurements against density profile from CT

1   analysis, and estimate the 3D distribution on main sites now stratigraphy from SMP

2   measurements surrounding test field.

3   The data can be used to drive forward models for emission and backscatter directly for the

4   date when measurements are available, providing a possibility to accurately study the effect of

5   small scale snow characteristics on emission and backscatter. As in the case of conventional

6   snow pit observations, most measurements were made outside of the instrument footprints.

7   However, as a one-time test during the third campaign period, SMP measurements and casted

8   CT samples were taken from an area in the test field observed by both *SnowScat* and *SodRad*

9   (Proksch et al., 2015). Data from IOPs are not a part of the NoSREx consolidated datasets but

10 can be made available on request from FMI.

3   NoSREx consolidated datasets

13   The key observations of NoSREx are collected in a consolidated dataset, providing easy access to

14 the main time series of *in situ* and microwave measurements. The data are provided as csv (comma

15 separated value) files and Excel spreadsheets. The data include

16 • Calibrated time series of *SnowScat* backscatter sigma nought at four incidence angles (30, 40,

17   50 60°) and three 2 GHz frequency bands (centre frequencies 10.2, 13.3 and 16.7 GHz). Separate

18   data files are provided for the two measurement sectors (sector 1 = main measurement sector;

19   sector 2 = adjacent sector). Data are provided as averages over the full azimuth scan range of

20   both sectors, with the exception that some azimuth directions have been removed from the sector

21   1 data to avoid experimental plate targets set in 2010. NOTE: *SnowScat* consolidated data for

22   the third campaign season (2011-2012) is limited to a period after January 20th, 2012, due to

23   observed anomalies in the backscatter data.

24 • Calibrated time series of *SodRad* brightness temperatures at 10.65, 18.7, 37 and 90 GHz, H and

25   V pol, at four incidence angles (30, 40, 50 60°). Average value and standard deviation of each

26   elevation scan provided. The 90 GHz receiver was replaced by a 21 GHz receiver from autumn

27   2011 onwards.

28 • Time series of selected automated in situ observations at the IOA, the main FMI-ARC

29   automated weather station (AWS), the Meteorological mast. Data provided as average values

30   over the scan times (three or four hours) of *SnowScat* observations. Recently, an updated version

31   with one hour averages has been made available.

32 • Summary of weekly and bi-weekly manual snow pit measurements at the IOA.

33

4   Overview of collected data from NosREx I to IV

The NoSREx campaign seasons each had each distinctive characteristics concerning weather conditions, snow structure, and soil conditions. All of these affected the resulting microwave signatures, which are discussed in this section.

4.1   Weather and snow conditions

The four winter seasons covered by NosREx are summarized in the following in terms of weather, snow and soil conditions. The distinctive characteristics of each season of NoSREx are collected in Table 3, showing also a comparison to the 30-year average in the Sodankylä region.

For the first season (NoSREx I), the early onset of permanent snow cover (Day of Year [DOY] 279) and mild temperatures were clearly linked to a delayed evolution of soil freezing. Melt-refreeze events in December also caused the formation of a crust at the bottom of the snowpack. The maximum measured SWE was slightly over the 30 year average, while based on snow pit observations, depth hoar was largely absent. The following season (NoSREx II) saw a sharp onset of soil freezing; at its maximum, the measured soil frost depth was over 2 meters on March-April 2011. The season saw harsh temperatures in early winter and a relatively thin snow cover, with a maximum SWE of only 165 mm, the lowest maximum value for the three years investigated. This caused rapid freezing of the soils as well as the formation of a distinct depth hoar layer in the snow, which is exhibited by the highest average estimated snow grain size. The average bulk snow density was also notably low (0.17 g/cm^3).

Despite late onset of permanent snow cover (DOY 329), the third season of observations (NoSREx III) saw the thickest snow cover of the campaign, with a maximum recorded SWE value of 240 mm, and the lowest penetration of soil freezing, the largest measured value being 120 cm. The early season was exceptionally mild in temperatures. The thermal winter begun later than during the previous two years, with a relatively thick snow pack already present. As a result, the development of soil frost was initially slow, and soil temperature remained at ~0°C well past the beginning of February (see Figure 2c), indicating residual free water in the top soil. Snow pit information indicated that the formation of depth hoar was very weak in the early the season, due to the small temperature gradient between the top and bottom of the snowpack. Despite the subjective nature of visual grain size estimates, it can be concluded that the average grain size of the snow was clearly smaller during NoSREx III than the preceding two seasons, largely due to the absence of large depth hoar crystals in the dataset.

The fourth season exhibited soil and snow conditions close to the 30-year average. Compared to preceding seasons, the estimates of snow grain size were on average the smallest after the third season ($E = 1.1$ +/- 0.3 mm), while the SWE maximum fell between the first and second seasons.

4.2   Microwave signatures against snow and soil conditions

Figure 2 presents the time series of observations for the four seasons of NoSREx, summarizing some of the microwave and *in situ* information available. Co-polarized (VV-polarization) backscatter measurements from the *SnowScat* instrument measured at 50 degree incidence angle are given for the three 2 GHz frequency bands available in the consolidated datasets (centre frequencies at 10.2, 13.3 and 16.7 GHz). Vertically polarized *SodRad* observations at 18.7 and 37 GHz, typically used for detection of snow water equivalent, are displayed for the same time periods. Selected *in situ* observations include snow depth (*SD*), air temperature (T_{air}), ground temperature (T_G), bulk averages of manually measured snow density (ρ_S) and bulk averages of visual estimates of snow grain size (*E*). The microwave instruments suffered from installation delays and malfunctions, which appear as data gaps in the autumn seasons of 2009, 2011 and 2012. Specialized tests and maintenance periods took place also in April 2010, April 2012 and February/March 2013. Notably, continuous measurements from snow free conditions to snow melt-off are available only for the second campaign season.

The microwave signatures reveal some interesting characteristics; in particular, the early snow season response was characterized by sudden decreases in backscatter, originating from snow melt events, followed by an increase in backscatter during refreezing. Several such periods occurred e.g. in the autumns of 2009 and 2010; for 2010, the same features can be observed in *SodRad* brightness temperatures. A distinct feature observed during the first, second and fourth seasons, was a gradual decrease of backscatter after the initial increase (measurements during the early winter of the third season, until January 2012, were lost due to an erroneous setting in the *SnowScat* instrument). The effect can be explained by the gradual relaxation of crust structures in snow, formed during the early season melt events, to more typical late-winter snow. The fact that the effect is more discernible at 16.7 GHz than at the two lower frequency bands implies that the feature is dominated by changes scatter in the snow volume. Unfortunately, the *in situ* data was not able to provide a quantitative measure of the phenomena, as objective measurements of the snow structure (e.g. computer tomography samples, see section 2.6) were not taken in the early season. Nevertheless, the observations are consistent with the expected backscatter behaviour of snow undergoing metamorphism.

Overall, there is very low response at X-band (10.2 GHz) to changing snow conditions during the entire snow season, with signatures during the first and third seasons showing even a continuous decreasing trend in backscattering intensity. The response at the low Ku band

1 (13.3 GHz) shows some increase in intensity during the first and second seasons (Figure 2a and

2 b), while during the third season (Figure 2c) no increase is apparent. A notable response at the

3 higher Ku-band (16.7 GHz) is observed for the first, second and fourth seasons. However, in

4 particular during the last season (Figure 2d), the increase in backscattering cannot be attributed

5 to increase in snow mass, as the measured snow height and density remained almost constant

6 from March to April 2013, when an increase of Ku band backscattering was observed. Rather,

7 the increase can be related to the observed increase in snow grain size.

8   The measured *SodRad* brightness temperature response showed clear similarities with the

9 backscatter measured by *SnowScat*. In particular, the dynamic responses of both the 18.7 and

10 37 GHz channels were strongest for the second season ((Figure 2b), and notable also for the

11 first season ((Figure 2a; note: early season dynamics not visible due to late start of

12 measurements). Signal dynamics at 37 GHz were much reduced during the third campaign

13 season (Figure 2c), indicating a low amount of total scattering in the snowpack, despite the third

14 year exhibiting the highest total SWE.

15   It should be noted that for the first and third campaign seasons, measurements were begun

16 only after the onset of snow cover. Furthermore, in November 2012, *SodRad* measurements

17 were halted due to maintenance immediately after onset of snow cover. The early season drop

18 of the 37 GHz brightness temperature is thus not apparent in the data for those seasons. The

19 *SodRad* instrument also malfunctioned in early April 2012, missing the last significant increase

20 in SWE of the season.

21   The small average E during NoSREx III (1.0 mm, compared to 1.4 and 1.5 mm for NoSREx

22 I and II, respectively) may explain in part the diminished dynamics of the backscatter and

23 emission signals observed during this season. The low bulk average value of E reflects mainly

24 the lack of a depth hoar layer during NoSREx III, whereas for NoSREx II a significant layer of

25 depth hoar was observed. For the first NoSREx season, large grains were prominent in the lower

26 snow layers due to early formation of melt-refreeze crusts.

27   A declining trend towards the late season can be observed in the 3rd order fit of E in particular

28 for the first and second campaign seasons (Figure 2a and b); this can be explained by newly

29 fallen layers of snow with a small grain size forming an increasingly large part of the total

30 snowpack, thus affecting the bulk average. For the fourth campaign season (Figure 2d), the

31 average grain size was observed to increase almost monotonously for the entire dry snow

32 season. This may explain why both the 16.7 GHz backscattering and 37 GHz emission

1 signatures continue to indicate increasing scattering in the snow, despite the snow height

2 remaining almost constant between March and April 2013.

3 **5 Model analysis**

4 To demonstrate the use of the NoSREx data in evaluation of microwave emission and

5 backscattering models, the MEMLS3&a model consisting of simulation of both active and

6 passive microwave response (Wiesmann and Mätzler, 1999; Proksch et al., 2015) was applied.

7 The expected backscatter and emission response against increasing SWE was simulated using

8 a one-layer configuration. Observations from the second campaign season (2010-2011) were

9 used as a reference.

10 With the exception of SWE, all model parameters were kept constant in simulations. Soil,

11 snow and air temperatures were set at -5 °C. Snow density was kept at 170 kg m^{-3}, which was

12 the average value measured during NoSREx II. In brightness temperature simulations,

13 downwelling sky brightness temperature (atmosphere + cosmic background) was estimated as

14 18 and 38 K for 18.7 and 37 GHz, respectively. Soil reflectivity was estimated based on early

15 season observations, resulting in vertically polarized reflectivity values from 0.015 to 0.03 and

16 horizontally polarized reflectivity values from 0.03 to 0.09, from 10.2 to 37 GHz, respectively.

17 For the active model, the specular part of the reflection was set at 0.75, and the cross-

18 polarization ratio was assumed as 0.1. The mean slope of surface undulations was set at 0.05.

19 The exponential correlation length required by MEMLS was not routinely measured during the

20 campaign, except for short campaign periods. Therefore, in these simulations, the correlation

21 length best fitting passive microwave simulations at vertical polarization was found iteratively,

22 using 18.7 and 37 GHz measurements at vertical polarization as a reference: the vertically

23 polarized emission was thought to be the least affected by the layered structure of snow cover.

24 The iteration resulted in a value of $p_{ex} = 0.25$ mm. The same value was then used in simulations

25 of emission at horizontal polarization, as well as simulation of backscattering. The correlation

26 length was measured using the SMP in February 2011, with the average value being 0.21 mm;

27 on the other hand, the average measured E during NoSREx II was 1.5 mm (see Figure 2b),

28 which following an empirical relation provided by Durand et al. (2008), would equally

29 correspond to $p_{ex} = 0.21$ mm. In order to visualize the effect of correlation length on simulations,

30 p_{ex} was varied by +/- 30 % to provide upper and lower bounds for model predictions. The

31 improved Born approximation was applied to simulate the scattering coefficient in MEMLS

32 (Mätzler and Wiesmann, 1999).

1   The result of the model run against *SnowScat* and *SodRad* observations is presented in Figure

2   3. As vertically polarized passive microwave observations were used to provide the model fit,

3   these can be seen to be mostly within the simulation bounds of p_{ex} +/- 30 %. For horizontal

4   polarization, the simulation provides an overestimation especially for higher values of SWE.

5   Using the same parameters, the active MEMLS3&a model reproduces well the *SnowScat* 10.2

6   GHz observations. On the other hand, the level of Ku band response is underestimated by

7   several dB. It is notable that using the baseline semi-empirical radiative transfer (sRT) model

8   developed for CoReH2O, the X-band response was typically overestimated while Ku band

9   response provided a good fit (ESA, 2012).

11   **6   Discussion**

12   Snow grain size, which presents the main source of information on snow microstructure for

13   NoSREx, is particularly difficult to establish in the field. Research also indicates that the grain

14   size by itself is insufficient to explain the full scattering behaviour of microwaves in snow (e.g.

15   Mätzler, 2002). The problem aggravates with snow particles of increasing size and complex

16   shape, as well as by sintering and clustering of snow grains. However, using data collected

17   during NoSREx, Leppänen et al. (2015) demonstrated that visually established grain sizes *E*

18   correlated with optical grain sizes measured using an objective measure of SSA. Furthermore,

19   Lemmetyinen et al. (2015) showed that an average grain size used to fit emission model

20   predictions captured both the magnitude and the seasonal trend of the visually estimated grain

21   sizes during NoSREx-II. Therefore, the information collected on *E* can be used at least as an

22   indicator of snow microstructural evolution during the NoSREx campaigns, even if not

23   employed directly in e.g. forward model simulations of emission and backscattering.

24   The NoSREx data has already proven useful for establishing novel relations between snow

25   properties and microwave signatures. Chang et al. (2015) applied the *SnowScat* observations

26   for comparisons of backscattering estimates using two derivations of the Dense Media

27   Radiative Transfer (DMRT), the bicontinuous model and quasi-crystalline approximations

28   (QCA). The bicontinuous approach is based on exact solutions of the Maxwell equations, while

29   QCA is an analytical approximation. Both approached showed reasonable agreement with

30   *SnowScat* observations collected during the second campaign season. Furthermore, Tan et al.

31   (2015) recently demonstrated the necessity of multiple scattering enhancement in DMRT, using

both active and passive observations from NoSREx for model evaluation. On the other hand, Leinss et al. (2015) applied *SnowScat* observations for differential interferometry, showing that the increase in SWE could be accurately obtained by exploiting the phase information retained in *SnowScat* observations. The high temporal resolution of *SnowScat* (three to four hours) allowed to mitigate decorrelation effects, while phase wrapping at the relatively high frequencies was addressed with a novel two-frequency approach. Data collected in the frame of NoSREx has also been exploited in recent studies focused on passive microwave signatures (e.g. Rautiainen et al., 2014; Pan et al., 2015).

7   Conclusions

The NoSREx campaign provides a near continuous time series of active and passive microwave signatures of seasonal snow cover in a natural environment over four winter seasons. The dataset is unique in providing signatures over several winter seasons from the same site, with each season exhibiting singular characteristics in both microwave backscattering and emission, as well as snow and soil properties. The dataset is freely available to science users (see Data availability).

Analysis of NoSREx datasets has already revealed several features of interest relating snow properties to the backscatter and emission, and the dataset has seen wide use in the field of developing advanced forward models for remote sensing observables in the microwave range. In particular, the collected data corroborate previous findings that correct determination of the snow microstructure is imperative for understanding microwave signatures. Future campaigns should increasingly make use of advanced methodologies for quantifying snow structural properties, including the snow microstructure. This will enable to develop new metrics relating snow properties to microwave signatures obtained from Earth Observing satellites.

Acknowledgements

The work was conducted under the European Space Agency project "Technical assistance for the deployment of an X- to Ku-band scatterometer during the NoSREx experiment" (ESA ESTEC contract 22671/09/NL/JA/ef). The staff at FMI-ARC are acknowledged for *in situ* data collection and operation of microwave instruments.

1 References

2 Barnett, T.P., Adam, J.C., & Lettenmaier, D.P., 2005. Potential impact of a warming climate

3 on water availability in snow-dominated regions. Nature, 438, 303-309.

4 Brasnett, B., 1999. A global analysis of snow depth for numerical weather prediction, J.

5 Appl. Meteorol. , 38, 726–740, doi:10.1175/1520-0450.

6 Chang, W., S. Tan, J. Lemmetyinen, L. Tsang, X. Xu, X., S. Yueh, 2015. Dense Media

7 Radiative Transfer Applied to SnowScat and SnowSAR. IEEE J Selected T. App. Earth Obs.

8 Remote Sens., 7(9): 3811-3825. doi: 10.1109/JSTARS.2014.2343519.

9 Derksen, C., and R. Brown, 2012. Spring snow cover extent reductions in the 2008-2012

10 period exceeding climate model projections. Geophys. Res. Lett., 39, L19504, DOI:

11 10.1029/2012GL05338.

12 Durand, M., E.J. Kim, and S.A. Margulis, 2008. Quantifying uncertainty in modelling snow

13 microwave radiance for a mountain snowpack at the point-scale, including stratigraphic effects.

14 IEEE Trans. Geosci. Remote Sensing, 46(6): 1753-1757.

15 ESA, 2012 Report for Mission Selection: CoReH2O, ESA SP-1324/2 (3 volume series),

16 European Space Agency, Noordwijk, The Netherlands.

17 Gallet, J.C., Dominé, F., Zender, C.S., & Picard, G., 2009. Measurement of the specific

18 surface area of snow using infrared reflectance in an integrating sphere at 1310 and 1550 nm.

19 The Cryosphere, 3, 167-182.

20 Groisman, P.Y., Karl, T.R., & Knight, R.W., 1994. Observed impact of snow cover on the

21 heat balance and the rise of continental spring temperatures. Science, 263(5144), 198-200

22 Kelly, R., A. Chang, L.Tsang, and J. Foster, 2003. A prototype AMSR-E global snow area

23 and snow depth algorithm IEEE Trans. Geosci. Remote Sens., 41(2), 230-242.

24 Leinss, S., A. Wiesmann, J. Lemmetyinen, and I. Hajnsek. Snow Water Equivalent of dry

25 snow measured by differential interferometry, 2015. IEEE J Selected T. App. Earth Obs.

26 Remote Sens., 8(8): 3773-3790.

27 Lemmetyinen, J., Derksen, C., Toose, P., Proksch, M., Pulliainen, J., Kontu, A., Rautiainen,

28 K., Seppänen, J., and Hallikainen, M., 2015. Simulating seasonally and spatially varying snow

29 cover brightness temperature using HUT snow emission model and retrieval of a microwave

30 effective grain size. Remote Sens. Environ., 156, 71-95.

Lemmetyinen, J., J. Pulliainen, A. Kontu, A. Wiesmann, C. Mätzler, H. Rott, K. Voglmeier, T. Nagler, A. Meta, A. Coccia, M. Schneebeli, M. Proksch, M. Davidson, D. Schüttemeyer, Chung-Chi Lin, and M. Kern, 2014. Observations of seasonal snow cover at X- and Ku bands during the NoSREx campaign. *Proc. EUSAR 2014*, 3-5 June 2014, Berlin.

Leppänen, L., A. Kontu, J. Vehviläinen, J. Lemmetyinen, and J. Pulliainen, 2015. Comparison of traditional and optical grain size field measurements with SNOWPACK simulations in a taiga environment. J. Glaciol., 61(225), 151-162.

Matzl, M. and M. Schneebeli, 2010. Stereological measurement of the specific surface area of seasonal snow types: Comparison to other methods, and implications for mm-scale vertical profiling, Cold Reg. Sci. Tech., 64, 1–8.

Matzl, M., & Schneebeli, M., 2006. Measuring specific surface area of snow by near-infrared photography. Journal of Glaciology, 52(179), 558-564

Mätzler, C., 2002. Relation between grain-size and correlation length of snow. Journal of Glaciology, 48(162), 461-466

Mätzler, C. and A. Wiesmann, 1999. Extension of the microwave emission model for layered snowpacks to coarse-grained snow. Remote Sens. Environ., 70:318-326.

Pan, J., M. Durand, M. Sandells, J. Lemmetyinen, E. J. Kim, J. Pulliainen, A. Kontu and C. Derksen (accepted). Differences between HUT snow emission model and MEMLS and their effects on brightness temperature simulation. IEEE Trans. Geosci. Remote Sens.

Proksch, M., C. Mätzler, A. Wiesmann, J. Lemmetyinen, M. Schwank, H. Löwe, and M. Schneebeli, 2015. MEMLS3&a: Microwave emission model of layered snowpacks adapted to include backscattering. Geosci. Model Dev., 8, 2611-2626.

Proksch, M., Löwe, H., & Schneebeli, M., 2015. Density, specific surface area, and correlation length of snow measured by high-resolution penetrometry. Journal of Geophysical Research: Earth Surface, 120, 346-362

Rautiainen K., J. Lemmetyinen, J. Pulliainen, J. Vehviläinen, M. Drusch, A. Kontu, J. Kainulainen, and J. Seppänen, 2012. L-band radiometer observations of soil processes in boreal and subarctic environments. IEEE Trans. Geosci. Remote Sens., 50(5): 1483-1497.

Rott, H., S.H. Yueh, D.W. Cline, C. Duguay, R. Essery et al., 2010. Cold Regions Hydrology High-resolution Observatory for Snow and Cold Land Processes. Proc. IEEE, 98(5): 752-765.

1   Schneebeli, M., and J. Johnson, 1998. A constant-speed penetrometer for high-resolution
2   snow stratigraphy, Ann. Glaciol., 26, 107 - 111.

3   Schwank, M., A. Wiesmann., C. Werner, C. Mätzler, D. Weber, A. Murk et al., 2010.
4   ELBARA II, an L-band radiometer system for soil moisture research. Sensors, 10: 584-612.

5   Takala, M., K. Luojus, J. Pulliainen, C. Derksen, J. Lemmetyinen, J-P. Kärnä, J. Koskinen,
6   and B. Bojkov, 2011. Estimating northern hemisphere snow water equivalent for climate
7   research through assimilation of space-borne radiometer data and ground-based measurements.
8   Remote Sens. Environ., 115(12), 3517-3529.

9   Tan, S., W. Chang, L. Tsang, J. Lemmetyinen, and M. Proksch, 2015. Modeling both Active
10   and Passive Microwave Remote Sensing of Snow Using Dense Media Radiative Transfer
11   (DMRT) Theory with Multiple Scattering and Backscattering Enhancement. IEEE J Selected
12   T. App. Earth Obs. Remote Sens.

13   Wiesmann, A., & Mätzler, C., 1999. Microwave emission model of layered snowpacks.
14   Remote Sensing of Environment, 70(3), 307-316.

Data availability

17   The NoSREx consolidated datasets are available after registration on the ESA Earth
18   Observations Campaign Data portal (https://earth.esa.int/web/guest/campaigns). *SnowSca*t raw
19   data are available for scientific use via FMI and Gamma remote sensing AG. Data from
20   NoSREx IOPs are available for scientific o request via WSL-SLF. The time series of SSA
21   profiles are available on separate request from FMI.

2   Table 1. *SnowScat* technical specifications.

Parameter	Value
Manufacturer	GAMMA Remote Sensing
Power:	230V, max ~ 60W
Weight:	~ 40 kg
Temperature Range:	-40° C to 40° C
Antenna:	dual pol, < 10° (3dB)
Antenna cross-pol iso:	< -20 dB
Frequency:	Stepped CW from 9.15 to 17.9 GHz
Incidence angle:	-40° to 110°
Azimuth angle:	-180° to 180°
Polarisation:	HH, HV, VV, VH
Dynamic range:	Receiver dynamic range > 80 dB with the 16 bit ADC
Signal bias:	< 0.5 dB

2   Table 2. *SodRad* technical specifications.

Parameter	Value
Manufacturer	Radiometer Physics GmbH
Power:	~300 W average, 500 W peak
Weight:	405 kg (including positioner)
Temperature Range:	-40° C to 45° C
Receiver & Antenna thermal stabilization	< 0.05 K
Antenna θ_{3dB}	< 6.1°
Antenna sidelode level:	< -30 dBc
Incidence angle:	30°< θ < 330°
Azimuth angle:	360°
Polarisation:	V and H
Frequencies:	10.65, 18.7, 36.5, 90 GHz
Bandwidth	400 MHz
System noise temperatures	< 900 K
Dynamic range:	0 – 350 K
System stability	1.0 K
Radiometric resolution	0.2 K RMS @1 s integration time

1   Table 3. Summary of seasonal characteristics for soil and snow conditions in winter periods of
2   2009-2010, 2010-2011 and 2011-2012, compared to 30-year average in the Sodankylä region.

	Season	30 -year average	2009-2010	2010-2011	2011-2012	2012-2013
Soil conditions	Onset of soil freezing (DOY)	298	289	289	320	298
	Date of maximum frost depth (DOY)	91	91	90	107	106
	Onset of soil thaw (DOY)	132	126	116	132	121
	Date of soil thaw (DOY)	148	141	152	147	146
	Max. frost depth (cm)	160	161	210	115	155
Snow conditions	Date of permanent snow cover (DOY)	299	279	300	329	289
	Date of SWE maximum (DOY)	109	88	72	112	102
	Date of snow melt onset (DOY)	Not available	90	92	115	102
	Date of snow melt-off (DOY)	129	134	128	140	133
	Max SWE (mm)	186.5 +/- 41.9 std (record min 120; record max 267)	225	165	240	191
	Average density (kg m⁻³)	Not available	200	170	190	200
	Grain size (Fiertz et al., 2009); depth-weight average +/- std (mm)	Not available	1.4 +/- 0.2	1.5 +/- 0.3	0.9 +/- 0.3	1.1 +/- 0.3
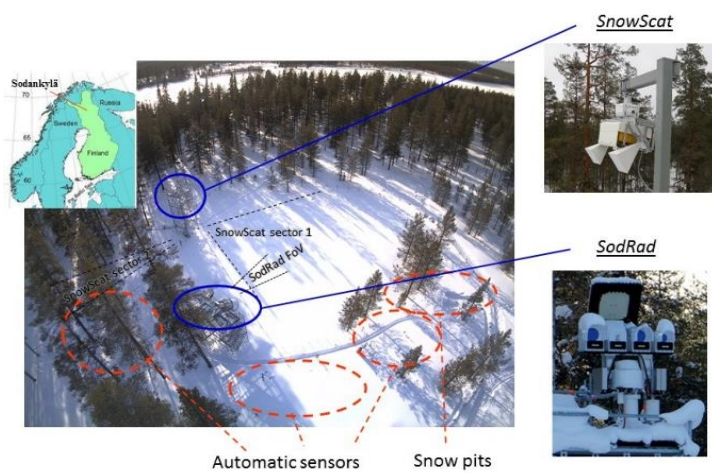
3   Figure 1. Webcam image of NoSREx IOA and photographs of main microwave instruments, the
4   *SnowScat* scatterometer and the *SodRad* radiometer system.
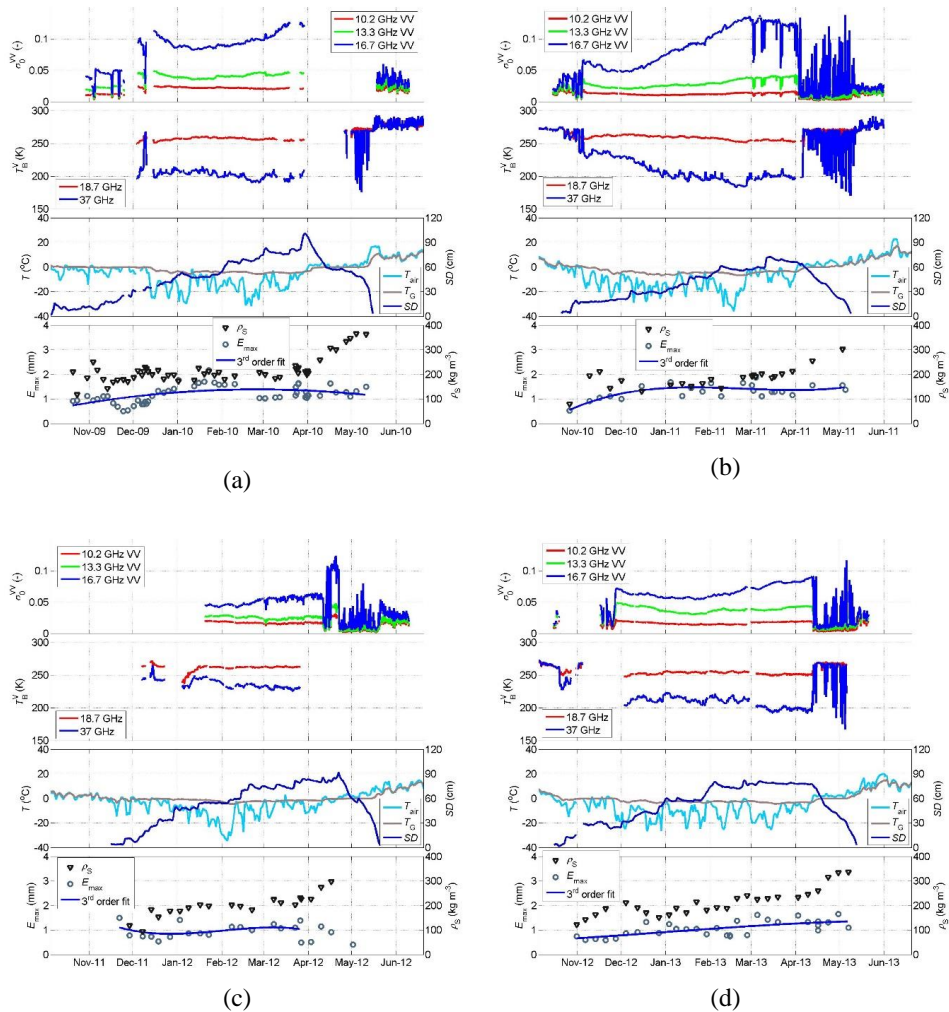
Figure 2. Summary of NoSREx seasons I-IV (a-d). Panels from *SnowScat* VV-polarized backscattering 50° incidence angle; *SodRad* brightness temperatures at 18.7 and 37 GHz, vertical polarization, 50° incidence angle; snow depth (*SD*), air temperature (T_{air}) and ground temperature (T_G); bulk averages of manually measured snow density (ρ_S) and visual estimates of snow grain size (*E*).
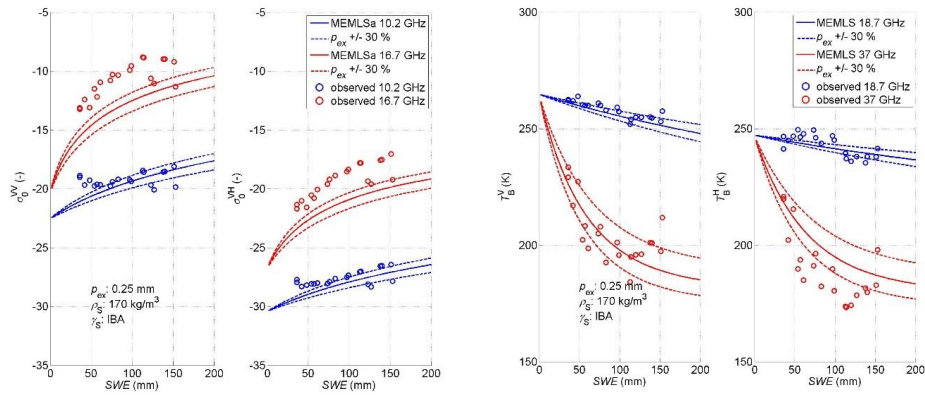
Figure 3. Comparison of modelled and measured response of backscatter (left) and brightness temperature (right) to increase in SWE during NoSREx II. Simulations in a one-layer configuration using MEMLS3&a (Wiesmann & Mätzler, 1999; Proksch et al., 2015) for 50 degree incidence angle. Scattering coefficient estimated using the Improved Born Approximation (IBA). Constant values of snow density (ρ_S) and exponential correlation length (p_{ex}) applied. Exemplary simulation error limits calculated by modifying p_{ex} by +/- 30%.